One-step calcination synthesis of rice husk biochar-doped g-C_3N_4 for efficient photodegradation of norfloxacin

Xiaodong Yang , Jin Zhao , Enshuo Zhang , Bowen Jiang , Shengjun Zhao , Tianyang Luo , Pengkai Sun , Shanlin Yang , Ye Han , Lili Wang , Fanming Zeng , Cheng Ding , Bin Gao

PII: S2772-4166(26)00250-0
DOI: https://doi.org/10.1016/j.hazadv.2026.101252
Reference: HAZADV 101252

To appear in: *Journal of Hazardous Materials Advances*

Received date: 9 October 2025
Revised date: 22 November 2025
Accepted date: 22 May 2026

Please cite this article as: Xiaodong Yang , Jin Zhao , Enshuo Zhang , Bowen Jiang , Shengjun Zhao , Tianyang Luo , Pengkai Sun , Shanlin Yang , Ye Han , Lili Wang , Fanming Zeng , Cheng Ding , Bin Gao , One-step calcination synthesis of rice husk biochar-doped g-C_3N_4 for efficient photodegradation of norfloxacin, *Journal of Hazardous Materials Advances* (2026), doi: https://doi.org/10.1016/j.hazadv.2026.101252

Highlights

- Rice-biochar/g-C_3N_4 photocatalyst was synthesized via one-step calcination method.
- BCN_5 achieved an NOR removal of 88.11%, approximately 1.51 times that of blank.
- BCN_5 exhibited a rate constant of 2.94×10^{-2} min^{-1} over 2 h under visible-light.
- Re-usable/stable BCN_5 could maintain 85.13% original performance after 5 cycles.
- Superoxide radicals contributed most to efficient NOR degradation of composite.

One-step calcination synthesis of rice husk biochar-doped g-C_3N_4 for efficient photodegradation of norfloxacin

Xiaodong Yang [a,1,*], Jin Zhao [a,1], Enshuo Zhang [a], Bowen Jiang [a], Shengjun Zhao [a], Tianyang Luo [a], Pengkai Sun [a], Shanlin Yang [a], Ye Han [a], Lili Wang [a,*], Fanming Zeng [b], Cheng Ding [c], Bin Gao [d]

[a] *Changchun University, No.6543 Satellite Road, Changchun 130022, China*

[b] *Changchun University of Science and Technology, No.7989 Satellite Road, Changchun 130022, China*

[c] *School of Environmental Science and Engineering, Yancheng Institute of Technology, Yancheng 224051, China*

[d] *Department of Civil and Environmental Engineering, Rensselaer Polytechnic Institute, Troy, NY 12180, U.S.A.*

[1] *The authors should be regarded as co-first authors.*

Corresponding authors (Xiaodong Yang; Lili Wang):

E-mail addresses: xiaodongyangccu@163.com; ccdxwll@163.com.

Abstract: Norfloxacin (NOR), a quinolone antibiotic contaminant, poses significant environmental and health risks. In this study, rice biochar-doped g-C_3N_4 (BCN) photocatalyst was fabricated via a one-step calcination approach. Substitution of bridged nitrogen with carbon atoms created delocalized π bonds, which acted as both physical bridges between atrazine ring and electronic conduits to facilitate charge transfer. Among the prepared catalysts, the BCN_5 composite demonstrated the greatest performance of NOR photocatalytic degradation, presenting a NOR removal efficiency of 88.11% with a rate constant of 2.94×10^{-2} min^{-1} over 2 hours under visible light, approximately 1.51 times that of pure graphitic carbon nitride (58.46%). It showed a promising reusability and stable properties, maintaining 85.13% of its original performance after five cycles. Mechanistic analysis identified superoxide radicals as a dominant substance affecting the degradation of NOR. This research highlights the potential of one-step synthesized rice husk biochar/g-C_3N_4 composites as an efficient, low-cost photo-catalyst applied in environmental remediation and water treatment.

Keywords: biochar; g-C_3N_4; photo-degradation; norfloxacin; antibiotic

1. Introduction

The discovery and use of antibiotics revolutionized medicine, significantly reducing mortality from infectious diseases. However, their excessive and indiscriminate use has led to severe environmental pollution (Geetha, 2025). Among various antibiotics, fluoroquinolone norfloxacin (NOR) is particularly concerning due to its widespread presence and persistence in the environment (Lan et al., 2024). NOR was commonly applied in healing bacterial infections of gram-positive/negative issues, leading to its frequent detection in wastewater and surface waters worldwide (Yang et al., 2024b).

Adsorption and photodegradation were cost-effective and reusable techniques applied in water treatment. Photocatalysis process generates electron-hole pairs, which can directly or indirectly degrade organic pollutants (Pawar et al., 2018). Common photocatalysts include TiO_2 (Schneider et al., 2014), g-C_3N_4 (Ong et al., 2016), Ag/Ag_2S/$BiFeO_3$ (Zhou et al., 2025), and AgBr/Bi_2WO_6 (Dong et al., 2025). G-C_3N_4 garnered much attentions as their exceptional optical properties, remarkable chemical stability, and facile synthesis (Wang and Wang, 2022). However, g-C_3N_4 photocatalysts still suffer from limitations such as a small surface area, high charge-recombination rate, and inadequate visible-light utilization (Ren et al., 2019). To optimize its photo-catalytic properties, various strategies have been explored, including development of diverse precursors, enhancement of surface area, doping various elements, or forming heterojunctions with other materials. For instance, g-

C_3N_4 synthesized from trithiocyanuric acid exhibited a large specific surface area (56.59 m^2/g), narrow bandgap (2.621 eV), and low carrier recombination rate, presenting a novel photo-degradation performance of diclofenac (Lu et al., 2023). Similarly, urea-synthesized g-C_3N_4 has shown high activation efficiency due to its wide bandgap and strong photoelectron density. Other studies have reported diverse productions of g-C_3N_4 using calcium carbonate as a hard template (Wang et al., 2015a) and nanoporous g-C_3N_4 via solvent heat treatment (Gu et al., 2015). Introduction of non-metallic elements such as phosphorus, boron, sulfur, oxygen, fluorine, iodine, and carbon was employed to optimize the photo-degradation properties of g-C_3N_4 (Cao et al., 2018; Hu et al., 2019; Hu et al., 2020; Huang et al., 2019; Wang et al., 2022; Yan et al., 2018). Additionally, transition metal ions like nickel, zinc, iron, cobalt, copper, and titanium have also been incorporated and to enhance the photocatalytic properties of g-C_3N_4 (Han et al., 2019).

In g-C_3N_4, carbon doping at bridging nitrogen sites leads to the formation of delocalized π bonds, increasing conductivity and narrowing the bandgap, thereby enhancing visible light absorption (Dong et al., 2012). Chen et al. developed a cost-effective method to synthesize carbon-rich g-C_3N_4, which exhibited significantly higher solar-driven ability of hydrogen production (Chen et al., 2018). Precursor self-assembly method to produce carbon-doped mesoporous g-C_3N_4 was illustrated and exhibited high efficiency for photocatalytic degradation of Rhodamine B (97%, 15 min) as well as photocatalytic reduction of CO_2 (60. 82 μmol/g, 5 h) (Jia et al., 2024).

Carbon-g-C_3N_4 nanotubes with increased rate of visible-light hydrogen production (1×10^4 μmol $h^{-1}g^{-1}$) was also synthesized and reported (Zhao et al., 2023).

Rice husk biochar, a byproduct of rice milling, is an abundant and sustainable carbon material. With global rice production estimated to reach 534.1 million tons by 2025, the large-scale production of rice husk biochar presents an opportunity for environmental applications. In particular, it can serve as a viable carbon source for elemental carbon incorporation. Biochar was more affordable than graphene and carbon nanotubes, and its manufacturing process was simple (Al Faruque et al., 2021; Aslam et al., 2021; Zhang et al., 2011). In this study, a simple and efficient approach to produce rice husk biochar-doped g-C_3N_4 composites via one step calcination synthesis was presented. Compared to conventional approaches, one step calcination method could achieve in-situ coupling of biochar formation and g-C_3N_4 synthesis, substantially simplifying the preparation process. The innovative technique not only overcome multi-processes but also increased production efficiency (Li et al., 2016; Shalom et al., 2013; Wang et al., 2015b). These composites exhibit superior photocatalytic performance and physicochemical stability compared to conventional catalysts, making them promising candidates for water treatment.

2. Materials and methods

2.1 Fabrication of composites

Rice-husk biochar (RB) doped g-C_3N_4 (CN) composites were prepared by one

step calcination method, placing 10 g of rice husk in an alumina crucible and heating it to 550 °C for 2 h. Residual biochar was finely ground and mixed with 10 g of urea, then mixture was heated in a muffle furnace (550 °C, 2 h) to obtain the composites named as BCN_x, while x represents various weight (0, 1, 2, 3, 4, 5, 6, and 7 mg) of rice husk biochar in composite.

The selection of biochar content (0-7 mg) was based on preliminary experiments and literature reports, which indicated that excessive carbon doping beyond this range would lead to defect accumulation and performance degradation. The 1 mg interval was chosen to precisely identify the optimal doping level.

2.2. Analysis and characterization methods

X-ray diffraction (XRD, Japan), X-ray photoelectron spectroscopic (XPS, USA), and Fourier transform infrared spectroscopy (FT-IR, IR-Tracer 100) was used to measure the crystalline, compositional, and surface functionality properties of composites, respectively. Their microstructure and element-distribution was determined using an scanning electron microscope (SEM-EDS, JSM-7500). Morphology of composites was observed using a transmission electron microscope (TEM). Surface charge, porosity, and photo-electrochemical properties of composites was evaluated by using a Zeta potential analyzer (Zeta, MALVERN ZSU3200), a gas sorptometer (JW-BK 200 C), and an electro-chemical workstation (CHI660E, Pt-Ag/AgCl electrodes, Na_2SO_4 electrolyte).

2.3. NOR Photocatalysis Experiments

NOR removal of composites was investigated by using a xenon lamp (300 W, Wavelength range: 380-780 nm, Microsolar 300). A 10 mg composite was poured into NOR solution (50 mL, 20 mg/L, ph=7, 25℃) and protected from light (30 min) to achieve an equilibrium, and then irradiated by the xenon lamp. The suspension was obtained every 20 min and measured using a UV-Vis spectrophotometer (Shimadzu UV-3600PLUS, Japan) at 274 nm.

2.4. NOR adsorption experiments

Add 10 mg of the composite material to NOR solution (50 mL, 20 mg/L) and incubate in the dark for 150 minutes. The suspension preparation time aligns with the photocatalytic reaction duration, and measurements are taken at 274 nm wavelength using a UV-visible spectrophotometer (Shimadzu UV-3600PLUS, Japan).

3. Results and discussion

XRD analysis was used to measure the crystalline properties in composite catalysts (**Fig. 1**). Both BCN_x composites exhibited typical g-C_3N_4 peaks at 13° and 27.4°, corresponding to a (100) and (002) plane, respectively. As shown in the figure, full width values of half maximum for (002) of BCN_x composites continuously decrease with increasing biochar content compared to that of pure CN, indicating weaken crystallinity of BCN_x composites. Obviously, the crystalline nature of g-C_3N_4 dominates over the amorphous characteristics of the biochar, resulting in the disappearance of the amorphous RB band at 22°.

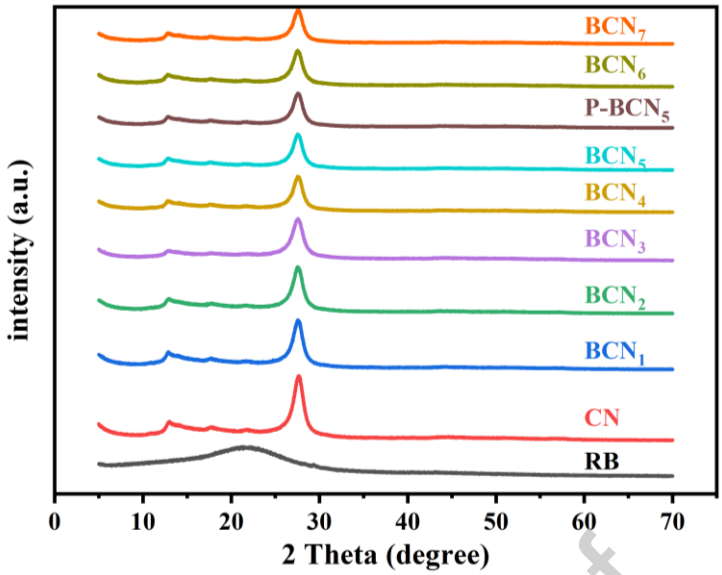

Fig. 1. XRD spectra of RB, CN, and BCN composites.

Rice husk biochar possessed a rough morphology with porous characteristics (Huong et al., 2020), while g-C_3N_4 illustrated a layered agglomerate structure in **Fig. 2a** and **b** (Yang et al., 2024a). Interestingly, BCN_5 composite exhibited a hierarchical stacking morphology and porous structure with various particles coated on surfaces (**Fig. 2c**), which are beneficial to its photocatalytic activity. TEM image of BCN_5 showed a typical 2D nanosheet and porous composite morphology in **Fig. 2d**, which was assigned to ammonia effects during a process of urea pyrolysis (Low et al., 2016). Amorphous biochar particles partially covered or grown on g-C_3N_4 nanosheets after heat treatment, forming a new composite microstructure of layer-porous characters. It is generally accepted that heterostructure can enhance photocatalytic efficiency by providing abundant active sites, shortening diffusion lengths, and weakening the recombination of electron-hole pairs (Cao et al., 2015). According to HRTEM results, a lattice stripe of 0.304 nm interplanar distance correspond to (002) lattice plane of g-C_3N_4 (**Fig. 2e**), confirming the successful one-step fabrication of

rice biochar-g-C_3N_4 catalyst. The surface charge of BCN_5 was -18.15 mV as determined from zeta potential analysis (**Fig. 2f**), which is close to that of CN (-18.65 mV). This similarity indicates that the addition of biochar components did not significantly change the surface electronegativity of resulting composites.

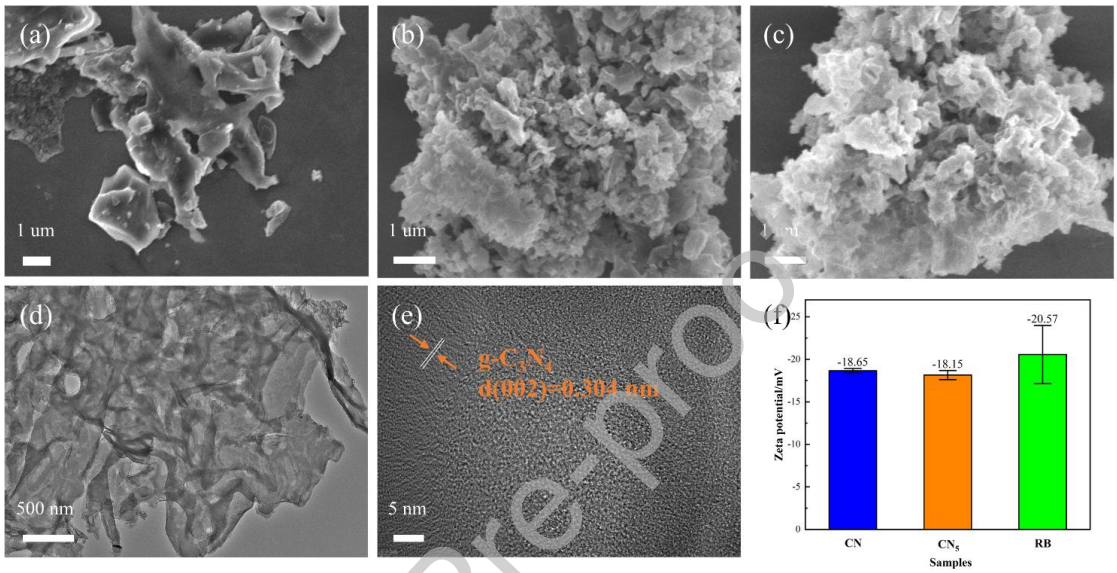

Fig. 2. SEM figures of (a) RB, (b) CN, and (c) BCN_5; (d) TEM and (e) HRTEM figures of BCN_5; and (f) Zeta chart of catalysts.

The FT-IR spectra confirmed a preservation of basic g-C_3N_4 molecular structure in biochar-dopped composites evidenced by the presence of several similar absorption peaks (**Fig. 3**). The FT-IR spectrum of RB exhibited a 1598 cm^{-1}peak of stretching vibration aromatic C=C, a 1091 cm^{-1} peak of C-O stretching vibration, and a 3441 cm^{-1} vibration peak for -OH bond (Kizito et al., 2015). The 809 cm^{-1} peak was assigned to breathing mode of s-triazine units in planar condensed carbon and nitrogen heterocycles. Stretching modes for CN heterocycles created the 1200-1700 cm^{-1} bands with peaks locating at 1251, 1410, 1560 and 1638 cm^{-1} (Fu et al., 2019). All the

composites exhibited a prominent peak of stretching vibration N-H bond in uncondensed amino groups and the O-H bond in physically adsorbed water or hydroxyl species when the wavenumber falls in the range of 2900 - 3600 cm^{-1}. Notably, the absorption intensity of 809 cm^{-1} peak in BCN_5 was relatively reduced compared to that of CN, probably attributed to partial replacement of nitrogen atoms by carbon atoms, further confirming successful carbon doping into the CN framework. Additionally, BCN_5 after degradation of norfloxacin (P-BCN_5) was also measured, their infrared peaks did not show any significant changes (Wei et al., 2024).

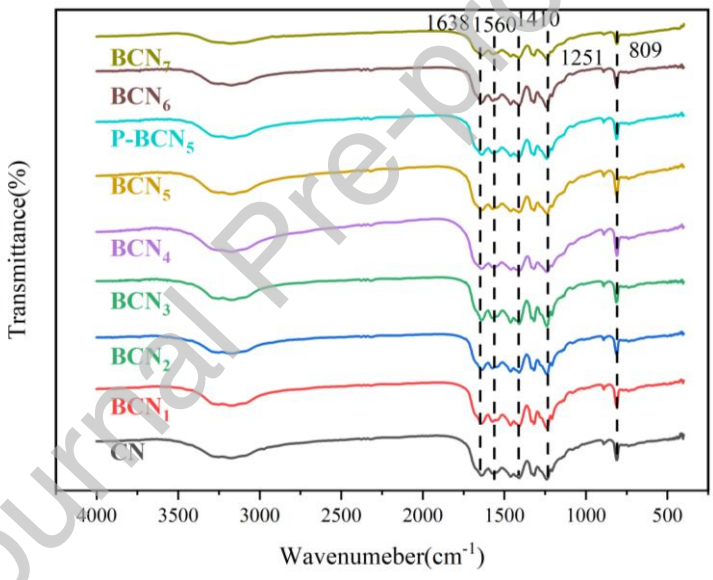

Fig. 3. FT-IR spectrogram of as-prepared BCN composites.

XPS was used to characterize chemical compositions and surface groups of catalysts. Based on XPS results, the molar ratios of C/N for CN and BCN_5 were calculated to be 0.78 and 0.83 (**Table S1**), respectively. It was inferred that the introduction of biochar significantly increased the exposure of carbon atoms within the g-C_3N_4 framework. C 1s XPS spectrum of BCN_5 exhibited typical 284. 8 and 288.

3 eV peaks, created by C=C/C-C and N-C=N bonds from N-containing aromatic rings, respectively (**Fig. 4a**) (Xiong et al., 2016). Intensity of the C=C peak in BCN_5 was relative high, indicating enhanced functionality of carbon-nitrogen structure due to the partial substitution of nitrogen atoms with carbon atoms. The main peaks of BCN_5 in the N 1s spectrum were located at 398.8, 400.3, 401.4, and 404.4 eV (**Fig. 4b**), corresponding to Sp^2-bonded N involved in a triazine ring (C=N-C), tertiary nitrogen group of $N-(C)_3$, amino group (C-N-H) originating from structural defects, and charging effect or positive charge localization within heterocycle, respectively (**Table S1**). Moreover, $N-(C)_3$ and (-C=N-C) peaks in BCN_5 exhibited higher intensities than those in pure g-C_3N_4, suggesting enhanced structural functionality in biochar doped g-C_3N_4 composites. In XPS survey spectra (**Fig. 4c**), a weak C-OH peak in O 1s, located at 532.5 eV, was assigned to oxygenated species (H_2O and CO_2) onto surface of catalyst (Che et al., 2019). The incorporation of carbon-atom can replace the bridging positions of nitrogen-atom in g-C_3N_4 structure, leading to newly generated delocalized π bonds (Wang et al., 2018).

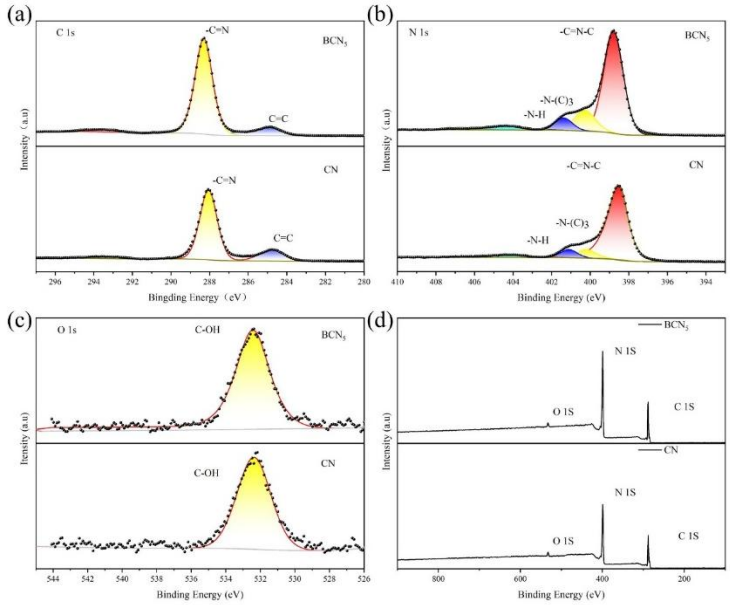

Fig. 4. High resolution (a) C 1s, (b) N 1s, (c) O 1s, and (d) complete survey XPS spectra of CN and BCN_5.

Therefore, key porosity parameters such as specific surface area (S_{BET}), BJH total pore volume (V_p), and mean pore size (L) were measured using nitrogen adsorption/desorption analysis (**Fig. 5**). RB possessed the largest specific surface area of 218 m^2/g (**Table S2**), with its pores predominantly consisting of micropores. Porosity of BCN_5 compared to g-C_3N_4 suggested that some biochar particles might have clogged the pores (**Table S2**). Furthermore, BCN_5 exhibited H3-type IV isotherms and hysteresis loops, indicating capillary condensation within its mesoporous structure.

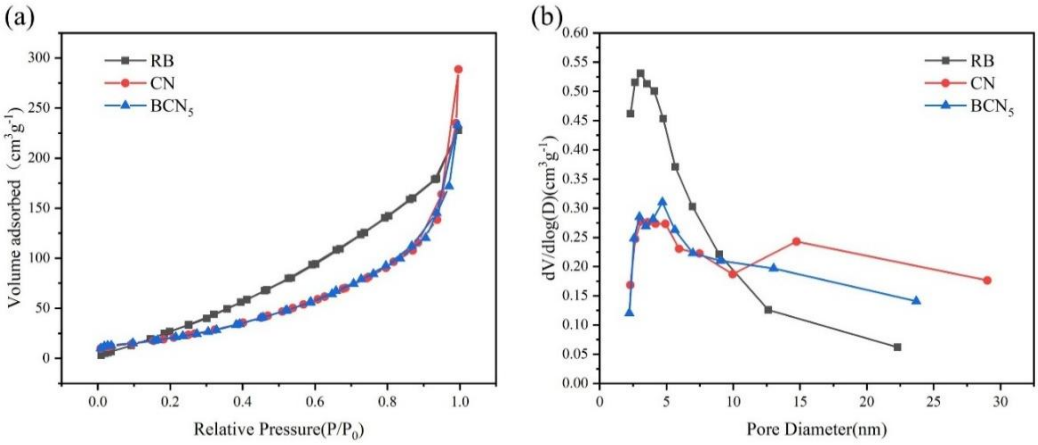

Fig. 5. (a) N_2 isotherms and (b) BJH pore-size distribution spectra of catalysts.

NOR photocatalytic degradation was carried out under the irradiation of 300 W xenon lamp ($\lambda > 400$ nm) after a 30-min dark adsorption-desorption equilibrium. The photocatalytic efficiency of NOR degradation over the BCN_5 catalyst was 88.11% after 120 min **(Fig. 6a)**, which increased almost 29.65% and became 1.51 times that of g-C_3N_4 (58.46%). Additionally, we tested the degradation efficiency of pure rice husk biochar, but rice husk biochar does not exhibit obvious photocatalytic properties. NOR removal efficiency of the composite catalyst was enhanced with increasing biochar content, with BCN_5 catalyst showed the best photocatalytic performance. Excessive incorporation of biochar, as shown in BCN_6 and BCN_7, led to a decline of NOR photodegradation ability. Over-occupation of C atoms may introduce excessive defects and facilitate charge carrier recombination, ultimately reducing the overall photocatalytic efficiency of the composites (Sun et al., 2023). To investigate NOR degradation mechanisms, Second-order kinetics (PSO) equation was selected to simulate the data and to describe photo-catalytic process. The obtained kinetic curves (**Fig. 6b**) and corresponding rate constants (K values, **Table S3**) for NOR removal by

different catalysts were obtained. Notably, the K value of pure g-C_3N_4 was 0.005 min^{-1}, while the addition of rice husk biochar components, the K value of BCN_5 catalyst gradually raised and reaching 0.029 min^{-1} almost 5.4 times that of the g-C_3N_4 catalyst. Subsequently, the K value decreased with further increases in biochar loading, with the BCN_7 catalyst exhibited a K value of 0.021 min^{-1}.

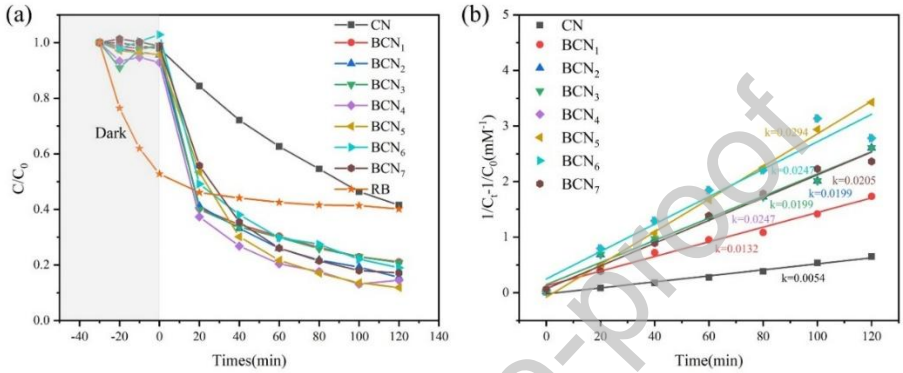

Fig. 6. (a) Photocatalytic removal and dark adsorption of NOR and (b) pseudo-first order kinetic simulations of NOR removal by photocatalysis.

While various samples were exposed to ultraviolet light as shown in **Fig. S1a**, the degradation performance of NOR notably decreased. Among the catalysts, BCN_5 exhibited the best performance of 36%, while CN showed the weakest performance of 9%. The composites almost exhibited no sorption capacities for norfloxacin **(Fig. S1b)**. To examine the statistical distribution characteristics of the obtained kinetic constant (k), we plotted the normal Q-Q plot of BCN_5, as shown in **Fig. S2**. The horizontal axis represented the experimentally measured k value, while the vertical axis displayed the quantile of the theoretical normal distribution. Those indicated that the vast majority of data points are tightly clustered around the reference line (y=x)

and fall within the 95% confidence interval. The normality test results confirm the good statistical properties of the k-value data, providing a reliable basis for subsequent quantitative comparison and analysis. In addition, we also used residual plots to validate the model, as shown in **Fig. S3**, the pseudo second-order model fits well.

Pure g-C_3N_4 showed significant absorption around the spectral edge of 449 nm (**Fig. 7a**), BCN_5 demonstrated an extended absorption edge at 453 nm, indicating a wider light absorption range. Apparent band gap was calculated following Tauc equation (Sun et al., 2019).

$$(\alpha h\nu)^2 = A(h\nu - Eg) \quad (1)$$

where α, E_g, and hν was the coefficient, band gap energy, and photon energy constant, respectively.

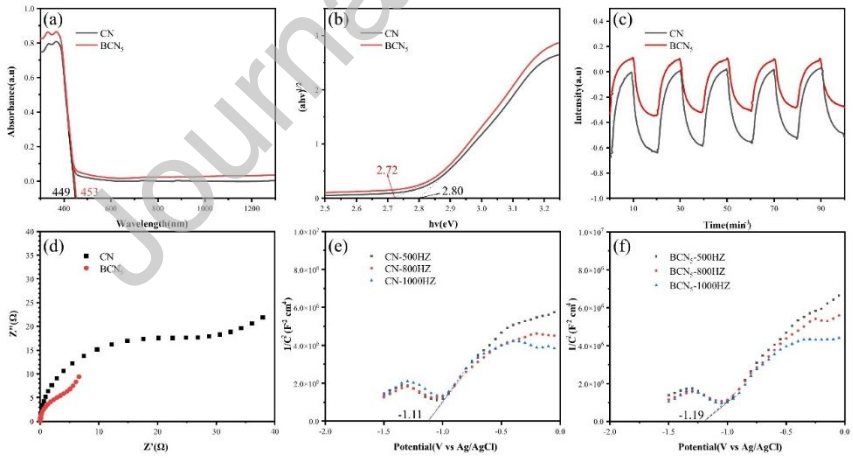

Fig. 7. (a) UV-Vis DRS, (b) $(\alpha h\nu)^2$ versus photon energy, (c) photoelectrochemical response, (d) EIS spectra of CN and BCN_5, and Mott-Schottky spectra of (e) CN and (f) BCN_5.

Compared to pure g-C_3N_4 (2. 80 eV,), the tangent interception of band gap energy

of BCN_5 was reduced to 2. 72 eV (**Fig. 7b**), indicating enhanced light absorption ability. Photocurrent densities and Nyquist plots were also measured. The variation in photocurrent density between electrodes demonstrated differences in efficiencies of photogenerated electron-hole separation (**Fig. 7c**). BCN_5 catalyst exhibited a relatively strong photocurrent response, indicating enhanced efficiency in separating photogenerated electron-hole pairs. Thus enhancing the efficiency of photocatalytic degradation of pollutants. (Jia et al., 2023). Furthermore, the EIS spectra (**Fig. 7d**) showed that BCN_5 had a small arc radius, and substitution of nitrogen with carbon probably increased electrical conductivity by facilitating the production of delocalized, extended π bonds (Dong et al., 2012), which may act as physical bridges connecting heptazine ring and promoting electron mobility. Mott-Schottky spectra was presented in **Fig. 7e** and **f**. Conduction band (CB) position of g-C_3N_4 and BCN_5 was -1.11 and -1.19 eV, while valence band (VB) position was calculated to be 1.69 and 1.53 eV, respectively, using following equation:

$$E_{CB} = E_{vB} - E_g \quad (2)$$

where E_g represents the structure of energy band.

In addition to investigate the contributions of different active substances in NOR removal of BCN_5, disodium ethylenediaminetetraacetic acid (EDTA), p-benzoquinone (P-BQ), and isopropanol (IPA) was used as scavengers of hole (h^+), superoxide radical ($\bullet O_2^-$), and hydroxyl radical (-OH), respectively. In the presence of IPA, EDTA, or p-BQ, NOR removal of the BCN_5 catalyst (88.11%) was reduced to 82.03%, 72.33%,

and 12.2%, respectively (**Fig. 8a**). The significant reduction of 75.69% in the presence of p-BQ indicated that superoxide radical was dominant active substance contributing to photocatalytic degradation of NOR. In addition, the decrease caused by EDTA (6.08%) and IPA (15.78%) treatments suggested that the hole and hydroxyl radicals were also involved in the degradation process. Therefore, through radical scavenging experiments, we found that superoxide radicals played a primary role in the degradation process, while hole radicals and hydroxyl radicals served as supplementary contributors. Piperazine ring conversion, decarboxylation, defluorination, and quinolone group conversion both contributed to NOR transformation into small-molecule substances and significantly reducing its environmental adverse effects (Gu et al., 2025).

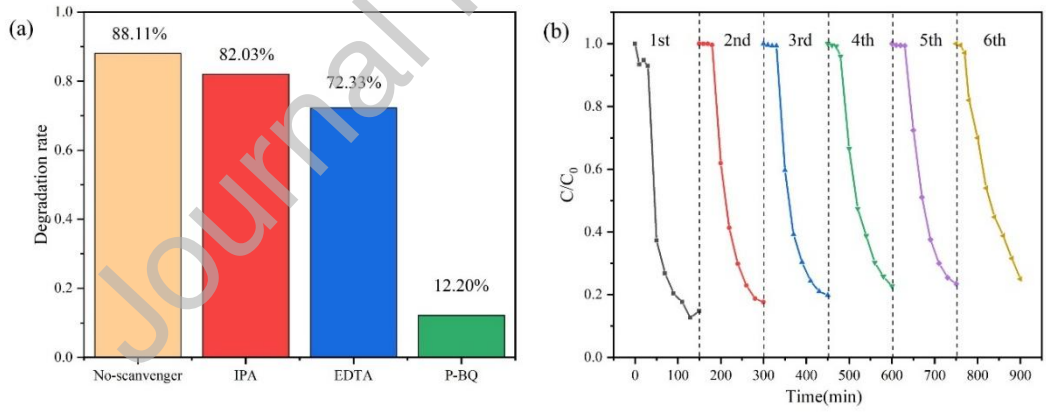

Fig. 8. (a) Free radical quenching experiment and (b) cycling experiment of BCN_5 to remove NOR antibiotic.

To further evaluate the cycling potential of BCN_5 for practical applications, a reusability test over five cycles was conducted. The NOR removal of BCN_5 after 5 regenerations was 75%, corresponding to a minor decrease of 13.1%, and still

retained 85.13% of its original performance (**Fig. 8b**). This indicates that the photodegradation of NOR by BCN_5 is relatively stable and durable. Based on the above findings, substitution of bridged nitrogen atom in CN structure by carbon atom through successful doping had several positive effects. For instance, formation of localized π states acted as electron mediators, accelerating charge transfer between neighboring heptazine rings. Moreover, by incorporating rice husk biochar, the bandgap was reduced, facilitating easier electron transitions.

Under visible light irradiation, the incorporation of biochar reduced the conduction band gap and accelerated electron mobility. These facilitated the electron transfer from the VB to the CB of BCN_5, thus gained more electrons and holes. Since potential of BCN_5's CB was more negative than the standard redox potential of O_2/-O_2^-, BCN_5 effectively reduced chemisorbed O_2 to -O_2^-. Holes directly degraded NOR molecules, and their consumption further accelerated electron-hole pair separation, thereby enhancing the efficiency of photo-degradation. The superoxide radicals, photogenerated holes, and hydroxyl radicals produced by light irradiation on the catalyst all possessed strong oxidative capabilities, promoting the photodegradation process. The improvement could be attributed to the fine incorporation of biochar into the framework of graphitic carbon nitride.

4. Conclusion

This study reported the positive effects of a facile one-step calcination method

for producing rice husk biochar-doped graphitic carbon nitride catalysts with highly efficient photo-degradation performance against NOR antibiotics. BCN_5 achieved a NOR removal efficiency of 88.11%, with a rate constant of 2.94×10^{-2} min^{-1} over 2 hours under visible light. This excellent performance was attributed to the reduced band gap and enhanced migration and separation of photogenerated carriers, with superoxide radicals as main active species. The photocatalytic performance of BCN5 was comparable to or better than many previously reported catalysts (**Table S4**). Its excellent reusability and stability suggest strong potential for practical water treatment applications. This work highlights the potential of the one-step calcination-synthesized rice husk biochar/g-C_3N_4 composite as an effective, low-cost, and environmentally friendly photocatalyst for environmental remediation and water treatment.

Acknowledgement

The authors truly acknowledged financial support from Jilin Provincial Natural Science Foundation (Free Exploration Project) of Jilin Provincial Science and Technology Development Plan (YDZJ202501ZYTS439), Jilin Province Development and Reform Commission (2024C017-1), and National Natural Science Foundation of China (12404492 and 22405263).

CRediT Authorship Contribution Statement

Xiaodong Yang: Writing-original draft, Writing-Reviewing and Editing; **Jin Zhao:** Investigation and Writing; **Enshuo Zhang:** Investigation; **Bowen Jiang:** Data curation; **Shengjun Zhao:** Software; **Tianyang Luo:** Validation; **Pengkai Sun:** Investigation; **Shanlin Yang:** Data curation; **Ye Han:** Investigation; **Lili Wang:** Reviewing and Editing; **Fanming Zeng:** Investigation; **Cheng Ding:** Reviewing and Editing; **Bin Gao:** Writing-original draft, Reviewing and Editing.

Appendix A. Supplementary data

E-supplementary data for this work can be found in on-line version of this paper.

References

Al Faruque, M. A., et al., 2021. A Review on the Production Methods and Applications of Graphene-Based Materials. Nanomaterials. 11**,** 2414.

Aslam, M. A., et al., 2021. Low cost 3D bio-carbon foams obtained from wheat straw with broadened bandwidth electromagnetic wave absorption performance. Applied Surface Science. 543**,** 148785.

Cao, S., et al., 2018. Sulfur-doped g-C_3N_4 nanosheets with carbon vacancies: General synthesis and improved activity for simulated solar-light photocatalytic nitrogen fixation. Chemical Engineering Journal. 353**,** 147-156.

Cao, S., et al., 2015. Polymeric Photocatalysts Based on Graphitic Carbon Nitride. Advanced Materials. 27**,** 2150-2176.

Che, H., et al., 2019. Control of energy band, layer structure and vacancy defect of graphitic carbon nitride by intercalated hydrogen bond effect of NO_3^- toward improving photocatalytic performance. Chemical Engineering Journal. 357**,** 209-219.

Chen, Z., et al., 2018. Gradual carbon doping of graphitic carbon nitride towards metal-free visible light photocatalytic hydrogen evolution. Journal of Materials Chemistry A. 6**,** 15310-15319.

Dong, G., et al., 2012. Carbon self-doping induced high electronic conductivity and photoreactivity of

g-C_3N_4. Chemical Communications. 48, 6178-6180.

Dong, W. R., et al., 2025. Synthesis of hydrochar-based AgBr/Bi_2WO_6 heterojunction photocatalyst using dopant element and its loading on PVDF membrane: Study on degradation of sulfadiazine. Separation and Purification Technology. 360.

Fu, J., et al., 2019. Ultrathin 2D/2D WO3/g-C3N4 step-scheme H2-production photocatalyst. Applied Catalysis B: Environmental. 243, 556-565.

Geetha, R., 2025. Environmental Impact of Ineffective Antibiotic Disposal: Strategies and Remedial Pathways: A Comprehensive Review. Environmental Quality Management. 34.

Gu, Q., et al., 2015. Template-free synthesis of porous graphitic carbon nitride microspheres for enhanced photocatalytic hydrogen generation with high stability. Applied Catalysis B: Environmental. 165, 503-510.

Gu, Q., et al., 2025. Effective periodate activation of direct Z-scheme g-C3N4/Cu2O heterojunction for photocatalytic norfloxacin degradation, anti-bacterial activity and toxicity assessment. Chemical Engineering Journal. 504, 159143.

Han, H., et al., 2019. A critical review of clay-based composites with enhanced adsorption performance for metal and organic pollutants. Journal of hazardous materials. 369, 780-796.

Hu, C., et al., 2019. Phosphorus-doped g-C_3N_4 integrated photocatalytic membrane reactor for wastewater treatment. Journal of Membrane Science. 580, 1-11.

Hu, X., et al., 2020. One-step synthesis of iodine-doped g-C_3N_4 with enhanced photocatalytic nitrogen fixation performance. Applied Surface Science. 510.

Huang, Y., et al., 2019. Controlling carbon self-doping site of g-C_3N_4 for highly enhanced visible-light-driven hydrogen evolution. Applied Catalysis B: Environmental. 254, 128-134.

Huong, P. T., et al., 2020. Novel activation of peroxymonosulfate by biochar derived from rice husk toward oxidation of organic contaminants in wastewater. Journal of Water Process Engineering. 33.

Jia, Y., et al., 2023. A facile synthesis of coral tubular g-C_3N_4 for photocatalytic degradation RhB and CO_2 reduction. Journal of Alloys and Compounds. 965.

Jia, Y. C., et al., 2024. Construction of carbon-doped mesoporous g-C_3N_4 catalytic nanoreactor via bubble template method for visible-light photocatalysis. Journal of Alloys and Compounds. 987.

Kizito, S., et al., 2015. Evaluation of slow pyrolyzed wood and rice husks biochar for adsorption of ammonium nitrogen from piggery manure anaerobic digestate slurry. Science of The Total Environment. 505, 102-112.

Lan, Y., et al., 2024. Cornstalk hydrochar produced by phosphoric acid-assisted hydrothermal carbonization for effective adsorption and photodegradation of norfloxacin. Separation and Purification Technology. 330, 125543.

Li, H., et al., 2016. Mesoporous graphitic carbon nitride materials: synthesis and modifications. Research on Chemical Intermediates. 42, 3979-3998.

Low, J., et al., 2016. Carbon-based two-dimensional layered materials for photocatalytic CO_2 reduction to solar fuels. Energy Storage Materials. 3, 24-35.

Lu, W., et al., 2023. A comparison study of photocatalytic performance of g-C_3N_4 prepared from different precursors for the activation of different peroxides. Separation and Purification Technology. 327.

Ong, W. J., et al., 2016. Graphitic Carbon Nitride (g-C_3N_4)-Based Photocatalysts for Artificial

Photosynthesis and Environmental Remediation: Are We a Step Closer To Achieving Sustainability? Chemical Reviews. 116, 7159-7329.

Pawar, M., et al., 2018. A Brief Overview of TiO_2 Photocatalyst for Organic Dye Remediation: Case Study of Reaction Mechanisms Involved in Ce-TiO_2 Photocatalysts System. Journal of Nanomaterials. 2018.

Ren, Y. J., et al., 2019. Interfacial engineering of graphitic carbon nitride (g-C_3N_4)-based metal sulfide heterojunction photocatalysts for energy conversion: A review. Chinese Journal of Catalysis. 40, 289-319.

Schneider, J., et al., 2014. Understanding TiO_2 Photocatalysis: Mechanisms and Materials. Chemical Reviews. 114, 9919-9986.

Shalom, M., et al., 2013. Improving Carbon Nitride Photocatalysis by Supramolecular Preorganization of Monomers. Journal of the American Chemical Society. 135, 7118-7121.

Sun, D., et al., 2019. Mesoporousg-C_3N_4/Zn–Ti LDH laminated van der Waals heterojunction nanosheets as remarkable visible-light-driven photocatalysts. International Journal of Hydrogen Energy. 44, 16348-16358.

Sun, J., et al., 2023. Biochar doped carbon nitride to enhance the photocatalytic hydrogen evolution through synergy of nitrogen vacancies and bridging carbon structure: Nanoarchitectonics and first-principles calculation. Carbon. 209.

Wang, H., et al., 2018. Carbon Self-Doped Carbon Nitride Nanosheets with Enhanced Visible-Light Photocatalytic Hydrogen Production. Catalysts. 8.

Wang, J., et al., 2015a. Environment-friendly preparation of porous graphite-phase polymeric carbon nitride using calcium carbonate as templates, and enhanced photoelectrochemical activity. Journal of Materials Chemistry A. 3, 5126-5131.

Wang, J. H., et al., 2015b. Environment-friendly preparation of porous graphite-phase polymeric carbon nitride using calcium carbonate as templates, and enhanced photoelectrochemical activity. Journal of Materials Chemistry A. 3, 5126-5131.

Wang, J. L., Wang, S. Z., 2022. A critical review on graphitic carbon nitride (g-C_3N_4)-based materials: Preparation, modification and environmental application. Coordination Chemistry Reviews. 453.

Wang, S., et al., 2022. Enhanced activation of peroxymonosulfate through exfoliated oxygen-doping graphitic carbon nitride for degradation of organic pollutants. Chemical Engineering Journal. 428, 131066.

Wei, M., et al., 2024. Electrolytic manganese residue-biochar composite for simultaneous removal of antimony and arsenic from water: Adsorption performance and mechanisms. Journal of Cleaner Production. 437, 140623.

Xiong, T., et al., 2016. Bridging the g-C_3N_4 Interlayers for Enhanced Photocatalysis. ACS Catalysis. 6, 2462-2472.

Yan, Q., et al., 2018. Facile synthesis and superior photocatalytic and electrocatalytic performances of porous B-doped g-C_3N_4 nanosheets. Journal of Materials Science & Technology. 34, 2515-2520.

Yang, X., et al., 2024a. Electrostatic self-assembly of hydrotalcite-based g-C_3N_4 composites for adsorption and photocatalytic degradation of aqueous norfloxacin. Journal of Environmental Chemical Engineering. 12, 114226.

Yang, X., et al., 2024b. Efficient removal of aqueous ciprofloxacin antibiotic by ZnO/CuO-bentonite composites synthesized via carbon-bed pyrolysis of bentonite and metal co-precipitation. Science of The Total Environment. 955**,** 176955.

Zhang, Q., et al., 2011. Carbon Nanotube Mass Production: Principles and Processes. ChemSusChem. 4**,** 864-889.

Zhao, S., et al., 2023. Controlling Electronic Properties of Carbon Nitride Nanotubes by Carbon Doping for Photocatalytic H_2 Production. Acs Applied Nano Materials. 6**,** 16231-16241.

Zhou, C. C., et al., 2025. Ag/Ag_2S plasmonic heterostructure promotes piezoelectric photocatalytic activity of $BiFeO_3$ nanofibers for degradation of ciprofloxacin and energy conversion. Journal of Environmental Sciences. 154**,** 212-225.

Funding Information

The authors truly acknowledged financial support from Jilin Provincial Natural Science Foundation (Free Exploration Project) of Jilin Provincial Science and Technology Development Plan (YDZJ202501ZYTS439), Jilin Province Development and Reform Commission (2024C017-1), and National Natural Science Foundation of China (12404492 and 22405263).

Graphical Abstract:

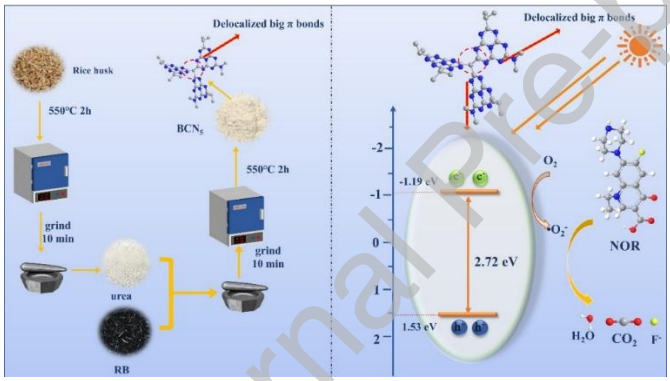

Declaration of interests

☒ The authors declare that they have no known competing financial interests or personal relationships that could have appeared to influence the work reported in this paper.